Highlights

Laboratory and field testing of a residential heat pump retrofit for a DC solar nanogrid

Aaron H.P. Farha, Jonathan P. Ore, Elias N. Pergantis, Davide Ziviani, Eckhard A. Groll, Kevin J. Kircher

- Off-the-shelf residential air-source heat pump retrofit to run on DC
- \bullet Experimental evaluation in psychrometric chambers and an occupied 208 m^2 test house
- Laboratory and field experiments show similar heat pump performance on AC and DC
- DC solar nanogrid model calibrated to empirical data from heat pump testing
- Model shows 12.5 to 16.7% annual electricity bill savings in DC vs. AC configuration

Laboratory and field testing of a residential heat pump retrofit for a DC solar nanogrid

Aaron H.P. Farha^a, Jonathan P. Ore^b, Elias N. Pergantis^{a,d}, Davide Ziviani^a, Eckhard A. Groll^a, Kevin J. Kircher^{a,c,e}

^aRay W. Herrick Laboratories, School of Mechanical Engineering, Purdue University, West Lafayette, IN, USA

^bEmerson Automation Solution, Pittsburgh, PA, USA

^cElmore Family School of Electrical and Computer Engineering, West Lafayette, IN, USA

^dTrane Technologies, Residential R⊗D Group, Tyler, TX, USA

^eCorresponding author,

Abstract

Residential buildings are increasingly integrating large devices that run natively on direct current (DC), such as solar photovoltaics, electric vehicles, stationary batteries, and DC motors that drive heat pumps and other major appliances. Today, these natively-DC devices typically connect within buildings through alternating current (AC) distribution systems, entailing significant energy losses due to conversions between AC and DC. This paper investigates the alternative of connecting DC devices through DC distribution. Specifically, this paper shows through laboratory and field experiments that an off-the-shelf residential heat pump designed for conventional AC systems can be powered directly on DC with few hardware modifications and little change in performance. Supporting simulations of a DC nanogrid including historical heat pump and rest-of-house load measurements, a solar photovoltaic array, and a stationary battery suggest that connecting these devices through DC distribution could decrease annual electricity bills by 12.5% with an after-market AC-to-DC heat pump retrofit and by 16.7% with a heat pump designed to run on DC.

Keywords: direct current, heat pumps, residential buildings, DC distribution, solar photovoltaics, batteries

1. Introduction

Residential buildings use over one-third of United States electricity [1]. Many large residential loads, such as motors that drive compressors, pumps, and fans, run natively on DC power [2, 3, 4]. Residential buildings are increasingly incorporating other large, natively-DC devices, such as solar photovoltaics (PV), electric vehicle chargers, and stationary batteries. Today, these natively-DC devices connect within buildings through AC distribution systems, requiring conversions between AC and DC at efficiencies that typically range from 85 to 95% [5]. Connecting natively-DC devices through DC distribution systems could reduce energy conversion losses, the installation and maintenance costs associated with inverters and rectifiers, and the use of materials such as copper and aluminum [6, 7].

While several modeling studies suggest that connecting DC devices within residential buildings through DC distribution could have significant benefits [5, 8], these studies often overlook key practical challenges associated with real-world implementation. Thus, experimental work is needed to convince decision-makers in business and government that DC technologies are worth bringing to market. Toward that end, Charalambous et al. investigated a hybrid AC-DC nanogrid connecting PV, a battery, and a heat pump in a small building meant to exhibit renewable energy technologies [9]. Charalambous et al. showed that reducing the number of AC-DC conversions raised PV self-consumption above 85% in a site study in Cyprus. Ore et al. switched a 14 kW (4 ton) heat pump to a 350 V DC source and ran steady-state laboratory cooling tests at maximum compressor speed following Air-Conditioning, Heating, and Refrigeration Institute (AHRI) Standard 210/240 [10]. Ore et al. estimated that switching the heat pump to DC could reduce input energy by 6 to 8%. Beyond heating and cooling, experimentalists have studied the switch to DC-driven light-emitting

diode lighting systems. For example, Sriram et al. [11] and Chacko et al. [12] showed that powering LEDs directly on DC could reduce input energy by up to 22%.

Complementing past experimental studies, this paper investigates the impacts of retrofitting a variable-speed residential air-source heat pump to run on $350~\rm V$ DC in both the laboratory and the field. The laboratory testing was conducted for both heating and cooling in a pair of psychrometric chambers that housed the heat pump's indoor and outdoor units, following AHRI Standard 210/240. The field testing was conducted in an occupied test house in West Lafayette, Indiana, during a winter month with outdoor temperatures as low as $-8.6~\rm ^{\circ}C$. To the authors' knowledge, this paper is the first to report laboratory results from retrofitting a variable-speed heat pump to run directly on DC for heating, or to report results from any type of DC heat pump testing in the field.

After reporting laboratory and field test results, this paper uses the field experiment data in system-level modeling of a DC nanogrid. The nanogrid includes 14.3 kW of solar PV, a 20 kWh stationary battery, and the heat pump with 14 kW (4 tons) of nameplate cooling capacity. The model uses one year of measured heat pump load data and rest-of-house load data from the test house, coincident solar irradiance measurements, and battery control logic that prioritizes direct use of solar power by the heat pump. Although the model does not include important effects such as voltage fluctuations, harmonics, stability, grid interaction, protection, or long-term reliability – important directions for future analysis – it builds upon existing modeling results by including more real-world load data and more realistic converter part-load efficiency curves. In simulations, the house's annual electricity bills are 12.5% to 16.7% lower with a DC nanogrid configuration than with an AC nanogrid configuration.

In summary, this paper makes three main contributions to the research literature. First, it presents the first laboratory test results for a DC heat pump retrofit that include both heating and cooling testing. Second, this paper presents the first field testing of any kind for a DC heat pump retrofit. Taken together, the laboratory and field test results build confidence that heat pumps can be retrofit to run reliably on DC without significant performance degradation. Third, this paper presents realistic modeling results that bring the research community one step closer to trustworthy quantification of the benefits of DC distribution systems in residential buildings.

This paper is organized as follows. Section 2 positions the contributions of this paper relative to past research. Section 3 details the methodology for laboratory and field experiments. Section 4 reports the results of the laboratory and field experiments. Section 5 presents the nanogrid models and simulation results. Section 6 discusses the results, the limitations of this paper, and possible directions for future work. Section 7 concludes the paper.

2. Related work

This section discusses DC power systems, focusing on low-voltage residential applications (Section 2.1). Section 2.2 then reviews related experimental research on residential DC equipment, focusing on heating and cooling. Section 2.3 surveys residential DC nanogrid modeling work. Section 2.4 positions this paper's contributions relative to past work.

2.1. DC power systems and the DC Nanogrid House

Electric power systems are commonly categorized by voltage as high (typically 50 kV or above), medium (1.5 kV to 50 kV), or low (below 1.5 kV). High-voltage DC transmission has the potential to enable power flows over longer distances with lower losses and higher capacity for a given conductor than high-voltage AC transmission [13], and has begun to see large-scale adoption [14]. Medium- and low-voltage DC power system technologies are somewhat less mature, but have potential applications in ships, trains, data centers, residential and commercial buildings, electric vehicle charging stations, and some heavy industries [6].

Medium- and low-voltage DC power systems may be configured as microgrids or nanogrids that can island a community or building, respectively, from the surrounding power system and serve local loads from local generation or storage. Controllable microgrids or nanogrids could improve resilience to extreme weather events and other emergencies by quickly islanding in response to outages in the surrounding power system





Figure 1: The DC Nanogrid House is a 1920s-era, 208 m², two-story, detached single-family house in West Lafayette, Indiana.

[15]. DC microgrids could alleviate issues faced by longer distance distribution of DC power [16, 17]. DC microgrids can also connect DC-powered devices through a common DC bus, increasing the throughput of power from source to sink by removing unnecessary conversions between AC and DC, with modeled energy savings of 10-15% [18, 19]. Relative to AC microgrids, DC microgrids could also reduce distribution line losses and provide better voltage regulation [19].

While DC microgrids and nanogrids could provide a range of benefits, they face several barriers to real-world adoption. DC distribution systems for residential and commercial buildings face a lack of cohesive standards and high capital costs [20, 6]. Protection for DC distribution systems in occupied buildings also presents challenges, as safely and reliably breaking an active DC circuit can be difficult [6], although recent innovations such as fault-managed power [21] might address protection issues. Installing and maintaining DC distribution systems can also entail higher costs and longer delays than AC systems, as electricians may have less experience with DC and appropriate DC equipment may not be commercially available [6].

Toward addressing some of these barriers to adoption, a team of researchers at Purdue University has renovated a test house with DC distribution and devices [22, 23, 24]. The DC Nanogrid House, shown in Figure 1, is a 1920s-era, 208 m², two-story detached single-family house occupied by three graduate student researchers. The house has been renovated with insulation, new windows, all-electric appliances, a 14.3 kW solar photovoltaic array, a 20 kWh stationary battery, and a custom home energy management system [25, 26, 27]. The house has both conventional AC wiring and a DC distribution system that is under ongoing development. After the retrofits described in this paper, the central variable-speed heat pump can now be switched between the AC and DC distribution systems through a lockout/tagout system. The project aims to retrofit additional devices – including an electric vehicle charging station, a full appliance suite, and lighting – to run on DC, with the ultimate goal of characterizing the performance differences between running a typical United Stateshouse on DC vs. AC. Retrofitting and testing the heat pump is an important step toward this long-term goal: The heat pump uses over two-thirds of annual energy in the house, which is located in a climate that sees both hot, humid, sunny summers and very cold winters.

2.2. Residential DC appliance experiments

Many works that discuss efficiency differences between AC and DC appliances only do so with modeling. The few experimental works of which the authors are aware considered small-scale appliances that operate at 48 V DC ([12, 11]). The only previous experimental publication that compared an at-scale test of a residential heat pump was also done in psychrometric chambers with the same heat pump evaluated in this paper [10]. That experiment was limited to cooling tests and did not evaluate the variable-speed functionality of the heat pump. The focus in [10] on cooling was likely due to the facts that air conditioning is much more prevalent than electric heating in North American housing, and that cooling loads align better with solar PV output, which peaks in the summer months. The heat pump was tested according to AHRI Standard



Figure 2: DC distribution deployments in the United States and Canada from 2022 [28]. Reproduced with permission.

210/240 conditions, but the setpoint of the heat pump was chosen such that the unit ran at full speed across the tests but was not explicitly controlled. Under these conditions, there was a 6-8% increase in system COP with DC power. Apart from Ore et al. [10], the authors are aware of no papers that directly compared AC and DC power inputs for a variable-speed residential heat pump.

In [28], Vossos et al. generated a map, shown in Figure 2, of DC projects (both small-scale demonstrations and full systems) in the United States and Canada as of 2022. Nearly all projects focus on lighting. The only heating or cooling system listed is the one tested by Ore et al. [10].

Beyond heat pumps, several studies have experimentally investigated efficiency improvements from powering smaller appliances on DC. Chacko et al. compared light-emitting diode bulbs and fans between AC and DC power, finding 20 to 40% energy savings from switching all lights and fans to DC [12]. Fregosi et al. [29] demonstrated 6-8% higher on-site PV consumption from powering light-emitting diode bulbs on DC. Fregosi et al. also modeled multiple building types across the United States, finding that increases in PV self-consumption were larger in sunnier states. Sriram et al. compared efficiency differences between powering light-emitting diode bulbs on AC vs. DC power-over-ethernet [11] in the DC Nanogrid House. They found that for small numbers of bulbs, fixed loads from power-over-ethernet networking equipment outweighed energy savings. When scaled up to all the bulbs in a typical house, however, savings more than offset networking loads, with net savings reaching up to 22%.

2.3. Residential DC nanogrid modeling

The device-level experiments surveyed above help build confidence that individual loads can function reliably on DC with equivalent or better performance than on AC. However, device-level experiments are insufficient to characterize the system-level benefits of connecting multiple DC devices through DC distribution. While system-level benefits could in principle be evaluated in hardware, it is challenging today to find appropriate DC distribution components (such as DC/DC converters and control systems) or loads that can connect directly to DC distribution without after-market retrofits. System-level modeling, while less realistic than field experiments, can provide preliminary estimates of system-level benefits and can explore implementation challenges and solutions.

Several studies have modeled the system-level benefits, such as reduced conversion losses, of DC nanogrids in residential buildings with rooftop solar PV [30, 31]. Frances et al. presented a range of options for modeling

Table 1: Summary of closely related studies on DC residential systems

Study	Year	Experiments?	Scope	Main results
[10]	2020	Yes	Heat pump in cooling	6–8% COP improvement
			mode	from DC
[11]	2024	Yes	Power-over-ethernet	≤20% lighting energy savings
			light-emitting diodes	from DC
[12]	2022	Yes	Light-emitting diodes,	20–40% energy savings from
			brushless DC fan motors	DC
[5, 34]	2014	No	PV and house loads in 14	5% energy savings from DC
. / 1			cities	without battery, 14% with
[30]	2010	No	PV and appliances	15% lower energy losses with
. ,				DC
[33]	2017	No	Market analysis	Few market-ready DC com-
				ponents
[35]	2025	No	Heat pump, battery, PV, wind	≤30% energy savings from predictive control

the efficiencies of different DC-DC, AC-DC, and DC-AC conversions [32]. Vossos et al. evaluated several residential microgrid or nanogrid architectures and applied simple efficiency calculations [5]. In follow-up work, Vossos et al. compared the nameplate efficiencies of commercially available products that offer both AC and DC options, showing that DC counterparts were often 20-30% more efficient [33]. Garbesi et al. estimated that a DC configuration can save 7 or 13% energy with or without energy storage, respectively [34]. Vossos et al. [5] and Garbesi et al. [34] both modeled space conditioning loads only for cooling; neither explored powering electric heating equipment on DC. Fapi et al. developed models to explore DC microgrid control with a PV array, a wind turbine, and a heat pump [35]. The PV array and wind turbine were modeled in detail, while the less detailed heat pump model assumed the coefficient of performance (COP) was a linear function of the outdoor temperature. Although Fapi et al. modeled a heat pump, they did not evaluate the energy savings from switching the heat pump from AC to DC. Table 1 summarizes these studies.

2.4. Contributions of this paper

In summary, this paper advances the state of knowledge on residential DC equipment and nanogrids in two main ways. First, this paper presents the first field demonstration that any major residential appliance – in this case, a heat pump, one of the largest energy users in electrified North American housing – can be readily retrofit and reliably operated on DC power. Expanding on prior work with the same heat pump [10], this paper also presents the first DC heat pump laboratory experiment results that include heating and variable-speed operation (rather than running steadily at maximum capacity). The laboratory and field experiments suggest that performance differences at the device level between AC and DC operation are statistically insignificant.

Second, this paper uses field data to model the system-level benefits of incorporating the tested heat pump into a DC solar nanogrid. While modeling a residential DC solar nanogrid is not new, to the authors' knowledge, this paper a) is the first to use real field data from a major appliance in a calibrated model, rather than relying on assumed performance parameters, and b) is the first to model DC heat pump operation year-round, including during peak heating conditions. The modeling suggests that, relative to an AC configuration, the DC configuration could reduce annual electricity bills by 12.5% to 16.7%. This is in line with previous research results, which typically show 10% to 20% energy savings [5, 34, 30].

3. Experimental methodology

An off-the-shelf variable-speed residential split-system heat pump with a scroll compressor and $14~\rm kW$ (4 tons) of nameplate cooling capacity was retrofitted to accept both AC and DC inputs. The unit was charged with 6.1 kg of R-410A to achieve 5 K of subcooling under the AHRI Standard $210/240~\rm A2$ conditions (Table 2) as per the manufacturer's specifications. To match the subcooling specification, the heat pump was run in steady state at the A2 test point (indoor chamber air: $27~\rm ^{\circ}C$ temperature, 51% relative humidity; outdoor chamber air: $35~\rm ^{\circ}C$, 40%) with an initial, uncalibrated mass of its refrigerant (R-410A). Incremental refrigerant was then gradually added until the measured refrigerant temperature at the outlet of the condenser coil was $5~\rm K$ cooler than the saturation temperature of the refrigerant at the measured condenser outlet pressure. The same subcooling calibration procedure was conducted before AC testing and before DC testing, allowing direct performance comparison.

Laboratory tests were performed in a pair of psychrometric chambers following AHRI Standard 210/240 [36]. For AC testing, power was supplied to the heat pump at a nominal split-phase 230 V AC. The DC configuration operated at a nominal bi-polar 350 V DC input. For both AC and DC testing, the auxiliary heating element was not present. Thermal and electrical performance was evaluated under variable-speed operation using the AHRI Standard 210/240 test procedures as shown in Table 2. To verify the testing procedures, an energy balance was calculated between the indoor unit refrigerant coil and the air blown across it to within 6% (Figures 7a and 7b).

Field tests were conducted at the DC Nanogrid House in West Lafayette, Indiana [24]. This is a "living laboratory" with three graduate student occupants. The house provides realistic boundary conditions for dynamic testing. A heat pump of the same make and model studied in the laboratory was installed. The refrigerant charge was calibrated to provide 5 K of subcooling in the A2 test condition. From the manufacturer recommendation, only the outdoor unit was retrofitted to run on DC. The outdoor unit (compressor, heat exchanger, and fan) uses more than 90% of the heat pump's overall energy. The indoor unit consists of heat exchanger, a fan for air circulation, and auxiliary electric resistance heating elements (large resistors) controlled by AC relays. The manufacturer stressed that attempting to power these AC relays on 350 V DC could present a fire risk, so the indoor unit was left on AC power. Future studies should investigate methods to retrofit heating element controls to run safely on DC. However, powering controlled heating elements on DC vs. AC should not change their energy use significantly. A DC retrofit should only affect the controls, which typically draw less than 1 W. Regardless of whether the heating elements themselves are powered on AC or DC, they should draw 5–20 kW for Joule heating.

3.1. Steady-state laboratory test descriptions

The heat pump was placed in a pair of psychrometric chambers to simulate indoor and outdoor conditions using AHRI Standard 210/240. Table 2 shows the steady-state test conditions for variable-speed unitary split residential systems.

The heat pump was instrumented with thermocouples and pressure transducers to directly measure the refrigerant and air properties. Laboratory data was collected using a National Instruments cRIO-2091 data acquisition system and the communication and data handling systems described in [37]. Figure 3 shows a piping and instrumentation diagram (adapted from [10]), which details the placement for cooling mode of the thermocouples, pressure transducers, and a Coriolis mass flow meter in the refrigerant cycle. Figure 4 shows a similar piping and instrumentation diagram for heating mode. The four-way valve in Figure 4 switches the heat pump to heating mode by reversing the direction refrigerant flow so that the indoor and outdoor heat exchangers function as the condenser and evaporator, respectively. Table 3 shows the refrigerant states, which are numbered the same for heating and cooling.

Table 4 shows types of sensors used and the associated measurement uncertainty ranges. Air dry-bulb temperature data was collected using three-by-three thermocouple grids at the inlet and outlet of the indoor unit. A chilled mirror dewpoint temperature humidity sensor was used to calculate the relative humidity at the outlet of the indoor unit. A capacitive relative humidity sensor was placed at the inlet to the indoor unit. The dry-bulb temperature and relative humidity were used to calculate an energy balance between the air and refrigerant as specified in AHRI Standard 210/240. Since the system is variable-speed,

Table 2: Test conditions from AHRI Standard 210/240

\mathbf{Test}	$\begin{array}{c} \textbf{Indoor} \\ \textbf{dry bulb} \\ [^{\circ}\textbf{C}] \end{array}$	$\begin{array}{c} \mathbf{Outdoor} \\ \mathbf{dry} \ \mathbf{bulb} \\ [^{\circ}\mathbf{C}] \end{array}$	$\begin{array}{c} \textbf{Indoor} \\ \textbf{RH} \\ [\%] \end{array}$	$egin{aligned} ext{Outdoor} \ ext{RH} \ [\%] \end{aligned}$
A2	27	35	51	40
B2	27	28	51	40
B1	27	28	51	20
$\mathbf{E}\mathbf{v}$	27	31	51	20
\mathbf{F}	27	19	51	40
H01	21	17	56	72
H11	21	8	56	72
H1n	21	8	56	73
H2v	21	2	56	82
H32	21	-8	56	70

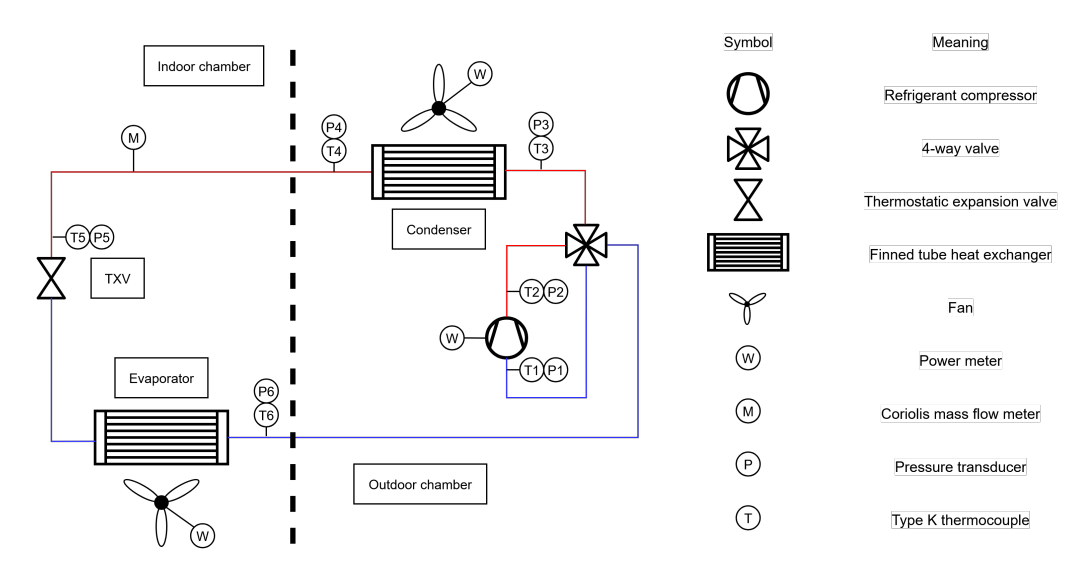


Figure 3: Piping and instrumentation diagram of the heat pump cycle in cooling mode.

the manufacturer provided a proprietary testing controller to operate the unit under the AHRI Standard 210/240 test conditions. This controller adjusts the revolutions per minute of the outdoor fan, indoor fan fan, and compressor.

Two sets of Watt transducers were required to gather data on the AC and DC configurations. The key difference between a DC and AC Watt transducer is the current measurement method, which is either through a Hall effect sensor (DC) or an inductive measurement (AC). For the AC configuration, three inductive Watt transducers were used to collect data from the total power to the indoor unit, the outdoor fan, and the compressor. The DC configuration used two Hall-effect Watt transducers to separately measure the power drawn by the indoor unit and the outdoor unit. The uncertainty of the power meters for the indoor fan and the outdoor fan were ± 5 W at full scale, while the outdoor unit power consumption was rated at \pm 12.5 W at full scale.

3.2. Dynamic field test descriptions

A heat pump of the same make and model tested in the psychrometric chambers was installed at the DC Nanogrid House in West Lafayette, Indiana. West Lafayette is in climate zone 5A, which typically sees 3,000

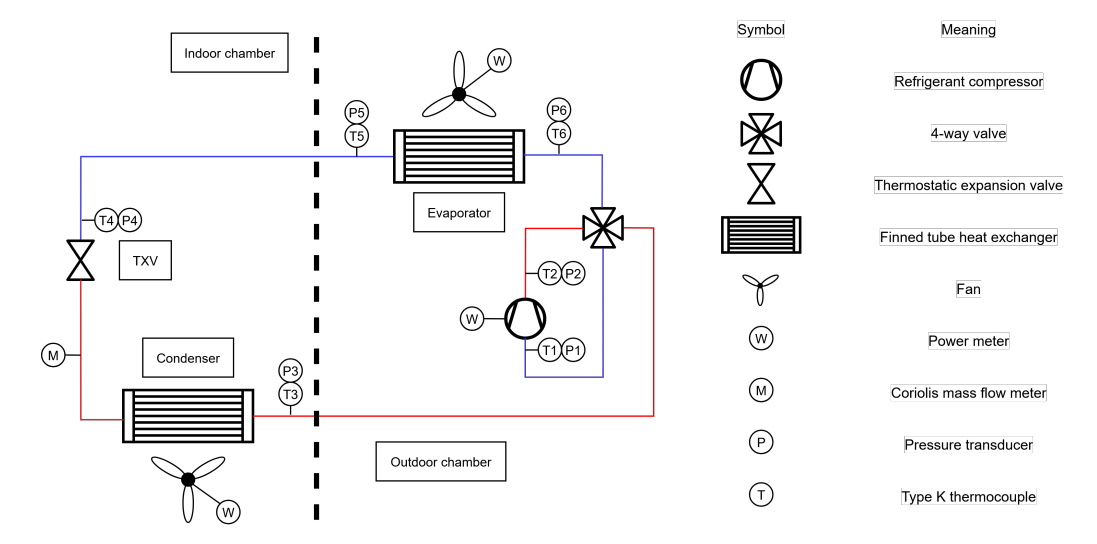


Figure 4: Piping and instrumentation diagram of the heat pump cycle in heating mode.

Table 3: State descriptions and measurements

State	Description	Measurement
1	Compressor suction	T,P
2	Compressor discharge	$_{\mathrm{T,P}}$
3	Condenser inlet	$_{\mathrm{T,P}}$
4	Condenser outlet	$_{\mathrm{T,P}}$
5	TXV inlet	$_{\mathrm{T,P}}$
6	TXV outlet	None
7	Evaporator inlet	None
8	Evaporator outlet	$_{\mathrm{T,P}}$

Table 4: Measurement uncertainty in the steady-state testing

Measurement	Uncertainty	Range	Manufacturer
Temperature	±0.5 K	[-200, 1260] °C	Type-K thermocouple
Pressure	$\pm 5~\mathrm{kPa}$	[0,7000] kPa	Dwyer Omega
Mass flow rate	$\pm 0.01~\mathrm{g/s}$	[0,600] g/s	Emerson
Indoor unit total power	$\pm 5~\mathrm{W}$	[0, 1000] W	Ohio Semitronics
Outdoor unit compressor power	$\pm 12.5~\mathrm{W}$	[0, 5000] W	Ohio Semitronics
Outdoor unit fan power	$\pm 5~\mathrm{W}$	[0, 1000] W	Ohio Semitronics

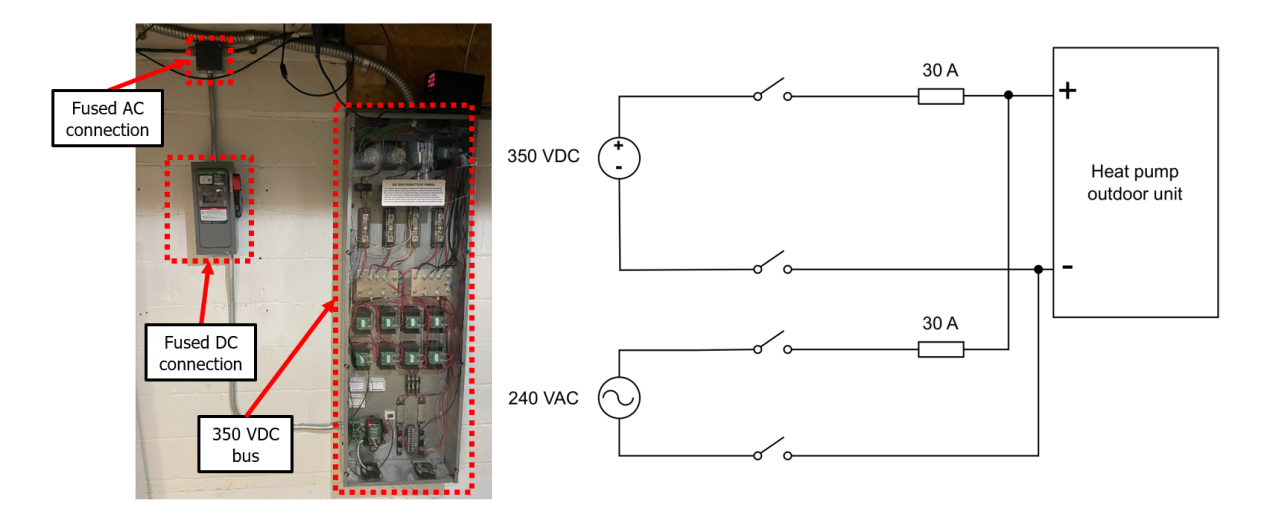


Figure 5: Wiring of the outdoor unit to the 350 VDC bus at the DC Nanogrid House using a lockout/tagout system.

to 4,000 heating degree-days per year (calculated using a balance-point temperature of 18 °C) [38]. The heat pump operated on a standard AC input from 2019 to 2024, when it was retrofitted to enable operation on AC or DC. A lockout/tagout system was implemented to enable manual switching between AC and DC. Figure 5 shows the physical installation and accompanying wiring diagram.

The heat pump was run with a constant indoor air temperature setpoint of 20.5 °C from December 18, 2024, through January 16, 2025. The power was measured from the on-board power transducers on the DC nanogrid's bi-directional inverter. The on-board power transducers are accurate to within ± 5 W. Historical AC data was directly measured with sub-metering on the breaker panel with sensors that are accurate to within ± 5 W.

The AC field data were measured one year prior to the DC field data, which could lead to somewhat higher performance estimates for AC than DC. Even under standard AC operation, heat pump performance can degrade from one year to the next due to machine wear and tear. Discussions with the manufacturer also suggested that the after-market DC retrofit was not ideal for this heat pump because the compressor's variable-speed drive was not designed to natively accept DC. Operating the compressor drive on DC could therefore accelerate performance degradation relative to AC operation.

The AC field data were selected from periods when the thermostat setpoint matched the 20.5 °C used for DC testing, and when weather conditions approximately matched the DC weather conditions. Figure 6 shows histograms of the daily average indoor-outdoor temperature difference for each day of the DC data (red) and the AC data (blue). More precisely, Figure 6 shows histograms of

$$\frac{1}{K} \sum_{k=1}^{K} \max(0, 20.5 \, ^{\circ}\text{C} - T_{\text{out}}(k)), \tag{1}$$

where the integer k indexes time steps, K is the number of time steps per day, 20.5 °C is the indoor air temperature setpoint, and $T_{\rm out}(k)$ (°C) is the outdoor air temperature. The $\max(0,\cdot)$ term in Equation (1) eliminates times when it is warmer outside than inside and heat demand is expected to be zero. While the AC and DC datasets in Figure 6 spanned nearly identical temperature ranges, the DC mean (dashed blue line) of 21.1 °C was 3.4 °C higher than the AC mean (dashed red line) of 18.7 °C. This indicates that the AC testing weather was somewhat warmer on average than the DC testing weather, which could lead to somewhat higher performance estimates for AC than DC.

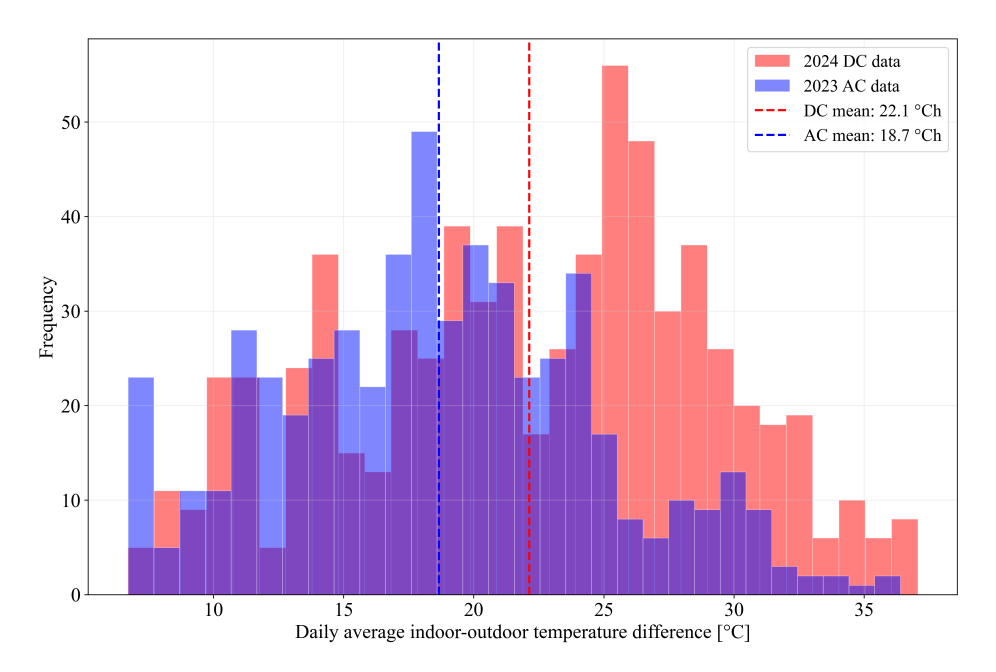


Figure 6: Histograms of daily average indoor-outdoor temperature difference for DC and AC testing. On average, AC field testing was conducted in somewhat warmer weather, which could lead to somewhat higher performance estimates.

4. Experimental results

4.1. Steady-state laboratory test results

Tables 5 and 6 show the heat pump's steady-state laboratory performance data on AC and DC, respectively. These tables include the test condition (from Table 2), the thermal capacity delivered by the unit, the indoor and outdoor power consumption, the total power consumption and the COP. The system COP was calculated as

$$COP = \frac{|\dot{Q}_{indoor} + \dot{Q}_{in,fan}|}{\dot{W}_{in,fan} + \dot{W}_{out,fan} + \dot{W}_{comp}},$$
(2)

where $\dot{Q}_{\rm indoor}$ (kW) denotes the rate of heat transfer from the refrigerant to the indoor air (positive in heating mode, negative in cooling mode), $\dot{Q}_{\rm in,fan}$ (kW) denotes the rate of heat transfer from the indoor fan to the indoor air (positive in both heating and cooling modes; assumed equal to $\dot{W}_{\rm in,fan}$), $\dot{W}_{\rm in,fan}$ (kW) denotes the indoor fan input power, $\dot{W}_{\rm out,fan}$ (kW) denotes the outdoor fan input power, and $\dot{W}_{\rm comp}$ (kW) denotes the compressor input power. The \dot{W} terms are all positive in both heating and cooling modes.

Figure 7 shows that refrigerant-side and air-side thermal capacity measurements agreed to within $\pm 6\%$ error under all test conditions on both AC and DC, as required by AHRI Standard 210/240. The AC test data had a mean absolute percent error of 4% between the refrigerant-side and air-side measurements. The DC test data had a mean absolute percent error of 2.5%. This builds confidence that thermal capacity was measured accurately.

Figure 8 shows that the thermal capacity measurements on DC agreed with the AC measurements to within $\pm 6\%$ error under all test conditions. The mean absolute percent error between AC and DC thermal capacity was 2.4% for cooling and 2.0% for heating. This suggests that the heat pump provides the same thermal capacity on DC as on AC.

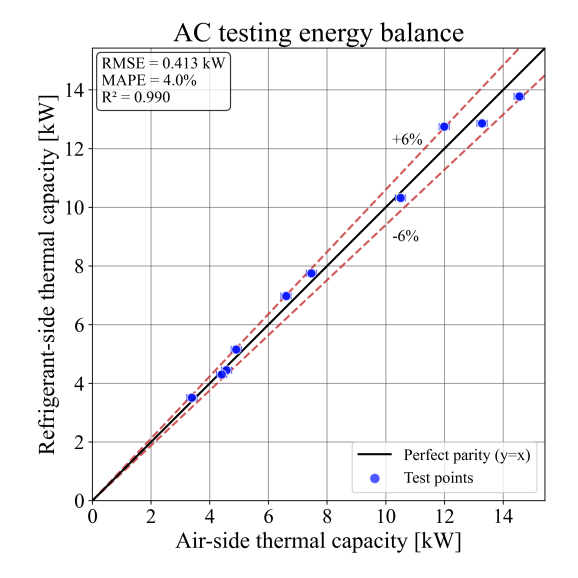
Figure 9 shows the AC and DC COP measurements vs. the temperature lift (meaning the difference between the measured condensing and evaporating temperatures for the refrigerant). The heat pump performed slightly worse (3–4% lower COP) on DC than on AC in low-load conditions, when the temperature lift was lower. By contrast, the heat pump performed slightly better (1–3% higher COP) on DC than on

Table 5: AC laboratory test results for AHRI Standard 210/240

Test	Thermal capacity [kW]	$\begin{array}{c} {\rm Indoor} \\ {\rm power} \\ {\rm [kW]} \end{array}$	$\begin{array}{c} {\rm Outdoor} \\ {\rm power} \\ {\rm [kW]} \end{array}$	Total power [kW]	COP [-]
A2	12.75	0.372	3.474	3.746	3.40
B2	13.78	0.211	3.038	3.155	4.36
B1	4.45	0.015	0.684	0.685	6.49
$\mathbf{E}\mathbf{v}$	7.75	0.092	1.416	1.471	5.27
\mathbf{F}	5.15	0.023	0.529	0.539	9.55
H01	4.30	0.072	0.660	0.705	6.09
H11	3.51	0.032	0.702	0.716	4.90
H1n	12.86	0.256	3.543	3.799	3.38
H2v	6.98	0.217	1.736	1.954	3.57
H32	10.32	0.572	4.292	4.865	2.12

Table 6: DC laboratory test results for AHRI Standard 210/240

	Thermal	${\bf Indoor}$	${f Outdoor}$	Total	
\mathbf{Test}	capacity	power	power	power	COP
	$[\mathbf{kW}]$	[kW]	$[\mathbf{kW}]$	[kW]	[-]
A2	12.44	0.272	3.293	3.565	3.49
B2	13.60	0.204	2.840	3.044	4.47
B1	4.57	0.028	0.716	0.744	6.14
$\mathbf{E}\mathbf{v}$	7.48	0.078	1.386	1.464	5.11
\mathbf{F}	5.03	0.033	0.517	0.550	9.15
H01	4.58	0.084	0.665	0.749	6.11
H11	3.56	0.040	0.714	0.754	4.72
H1n	12.78	0.383	3.374	3.757	3.40
H2v	6.98	0.214	1.727	1.941	3.60
H32	10.49	0.544	4.241	4.785	2.19



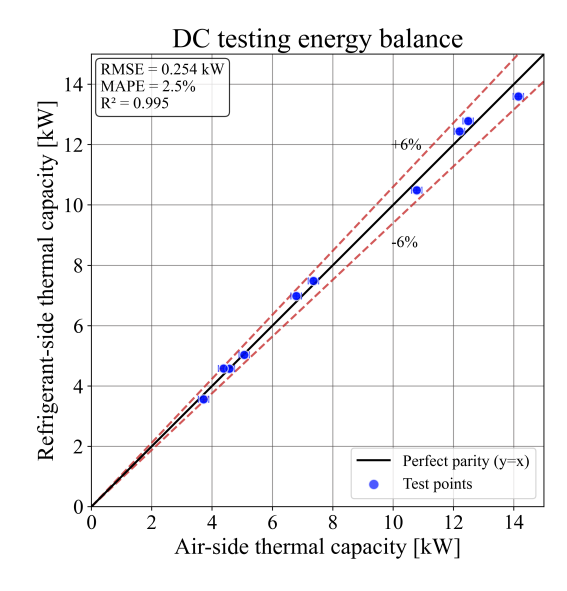


Figure 7: Air- and refrigerant-side thermal capacity measurements agreed to within $\pm 6\%$ error on AC (left) and DC (right).

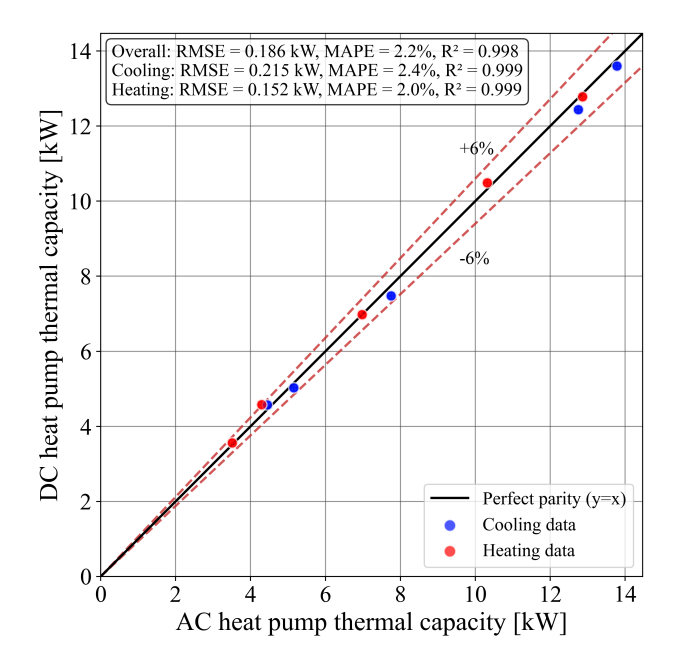


Figure 8: AC and DC thermal capacity measurements agreed to within ±6% for both heating (red) and cooling (blue).

AC during high-load conditions, when the temperature lift was higher. However, the relative measurement uncertainty was larger in low-load conditions because the absolute measurement uncertainty ranges were independent of the measurement magnitudes. For example, the outdoor unit power meter was accurate to within ± 12.5 W. This is 0.25% relative uncertainty at a high-load condition where the outdoor unit draws 5 kW, but 4.2% relative uncertainty at a low-load condition where the outdoor unit draws 300 W. The error bars in Figure 9, which were calculated from the measurement uncertainty ranges in Table 4, are therefore more pronounced at low temperature lifts than at high temperature lifts.

4.2. Dynamic field test results

Figure 10 shows the outdoor unit's hourly average input power vs. the hourly average indoor-outdoor temperature difference, calculated using Equation (1), for AC (blue) and DC (red) testing. The indoor-outdoor temperature difference is a reasonable stand-in for heat demand, which for most buildings scales approximately linearly with the temperature difference between the indoor and outdoor air. Figure 10 also shows quadratic fits and 90% Gaussian confidence intervals. The heat pump appears to draw slightly less power on DC than on AC for both low and high temperature differences. For intermediate temperature differences, the heat pump appears to draw slightly more power on AC than on DC.

Figure 11 shows outdoor unit's daily average input power vs. the daily average indoor-outdoor temperature difference for AC and DC. Figure 11 also shows linear fits and 90% Gaussian confidence intervals. The R^2 values for the AC and DC fits are 0.895 and 0.931, respectively. The AC fit likely has a higher R^2 value because there are more AC data at low indoor-outdoor temperature differences. This is because the weather was somewhat warmer during AC testing than DC testing. DC testing included more very cold days, and the associated data points tend to increase the slope of the DC best-fit line. Although there were slight performance differences on AC and DC power in field, the overlapping confidence intervals suggest that the performance differences are difficult to distinguish from the measurement uncertainty ranges.

A statistical hypothesis test was conducted to formally evaluate whether the field data indicate that the heat pump performed differently on AC vs. DC. The hypothesis test involved the weather-normalized daily average input powers on AC and DC,

$$X_a = \frac{P_a}{\Delta T - c}, \ X_d = \frac{P_d}{\Delta T - c},\tag{3}$$

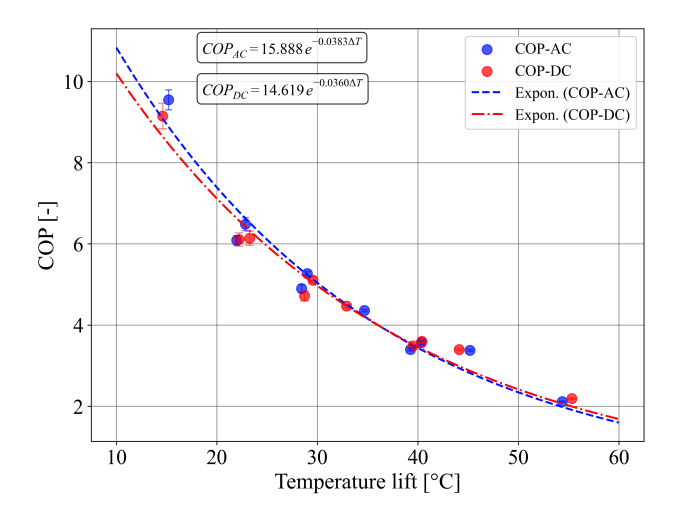


Figure 9: COP as a function of the temperature lift across all steady-state test conditions.

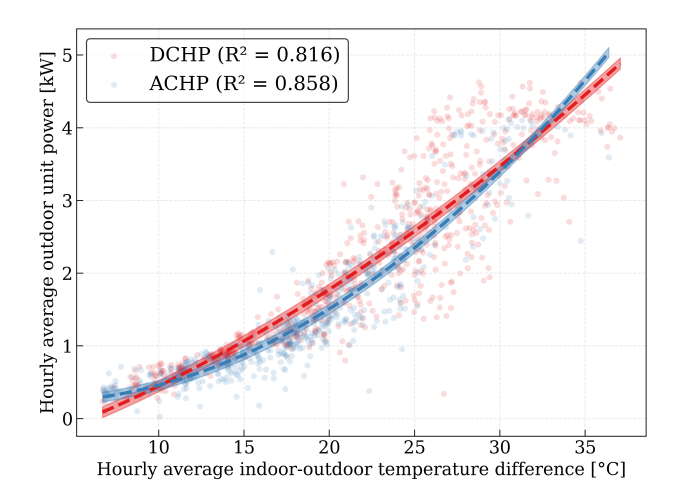


Figure 10: Hourly average outdoor unit input power vs. hourly average indoor-outdoor temperature difference.

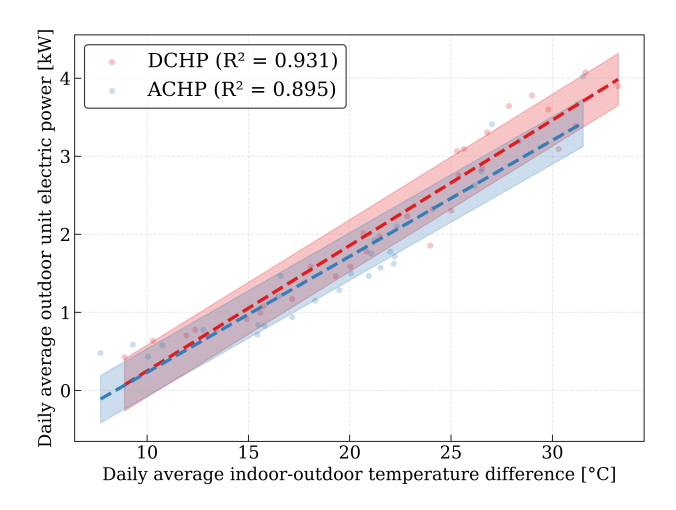


Figure 11: Daily average outdoor unit input power vs. daily average indoor-outdoor temperature difference. With a 90% confidence interval, the plots nearly overlap.

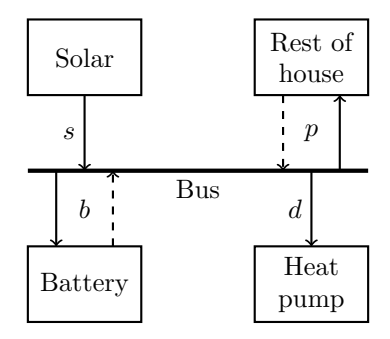


Figure 12: Power flows in the nanogrid include the solar output s, battery charging (or if negative, discharging) b, and heat pump input d. From a power balance on the bus, the nanogrid exports (or if negative, imports) p = s - d - b to (or from) the

where P_a (kW) and P_d (kW) are the daily average input powers on AC and DC, respectively, ΔT (°C) is the daily average indoor-outdoor temperature difference, and c=8 °C is the indoor-outdoor temperature difference at which heat demand is approximately zero. The random variables X_a and X_d were modeled as independent and Gaussian with potentially different means and variances. Each $(\Delta T_a, P_a)$ observation on AC gave rise to a realization of the corresponding random variable X_a , and similarly for DC. The null and alternative hypotheses were

$$H_0: \mu_a = \mu_d, \ H_1: \mu_a \neq \mu_d,$$
 (4)

where μ_a and μ_d are the population means of X_a and X_d , respectively. Under this model, the hypothesis test was a two-sample two-tailed Welch's unequal variance t-test with test statistic

$$t = \frac{\bar{X}_a - \bar{X}_d}{\sqrt{s_a^2/N_a + s_d^2/N_d}}.$$
 (5)

Here \bar{X}_a and \bar{X}_d are the sample means, s_a^2 and s_d^2 are the unbiased sample variances, and N_a and N_d are the sample sizes.

The hypothesis test results were computed in Python using the SciPy package's ttest_ind function with the $equal_var = False$ option. The resulting p-value, meaning the probability that the difference in sample means is greater than or equal to the observed difference, assuming the population means are equal, was 0.18. Because 0.18 > 0.05, the hypothesis test indicates that the difference in weather-normalized daily-average input powers on AC vs. DC was not statistically significant at a significance level of $\alpha = 0.05$.

5. System-level nanogrid modeling

This section presents the general nanogrid model equations and control logic (Section 5.1), the simulated AC and DC nanogrid configurations (Section 5.2), and the simulation results (Section 5.3).

5.1. General nanogrid model

Figure 12 shows the general nanogrid architecture, which includes solar PV, a stationary battery with energy and power capacities $\bar{x} = 20$ kWh and b = 12.5 kW, respectively, an heat pump, and a bidirectional connection to distribution system that serves the rest of the house. These components are all connected on a common bus. The solar power output s > 0 (kW) is injected to the bus. The battery's electric charging (or if negative, discharging) power b (kW) is extracted from (or injected to) the bus. The heat pump's electric power d > 0 (kW) is extracted from the bus. From a power balance on the bus, the power that the nanogrid exports to (or if negative, imports from) the rest of the house is p = s - b - d (kW).

The battery is modeled as a first-order linear dynamical system governed by the ordinary differential equation

$$\frac{\mathrm{d}x(t)}{\mathrm{d}t} = -\frac{x(t)}{\tau} + u(t),\tag{6}$$

Table 7: Solar array characteristics from the DC Nanogrid House

Sub-array	${f Tilt} \ [{f deg}]$	${\bf Azimuth} \ [{\bf deg}]$	Modules [#]
1	32	90	3
2	50	180	3
3	32	90	6
4	30	270	30

where t (h) denotes time, x (kWh) is the chemical energy stored in the battery, the self-dissipation time constant is $\tau=1600$ h (a reasonable value for lithium-ion batteries), and u (kW) is the chemical charging (or if negative, discharging) power. Assuming the charging power is piecewise constant over each discrete time step of duration $\Delta t=1$ h, the battery dynamics (6) discretize exactly to

$$x(k+1) = ax(k) + (1-a)\tau u(k), \tag{7}$$

where the integer k indexes discrete time steps and $a = \exp(-\Delta t/\tau)$. The electrical charging power b (kW) is modeled as a piecewise linear function of the chemical charging power:

$$b(k) = \begin{cases} \eta u(k) & \text{if } u(k) \le 0\\ u(k)/\eta & \text{if } u(k) > 0 \end{cases}$$

= \text{max}(\eta u(k), u(k)/\eta),

where $\eta=0.95$ is the battery's charging and discharging efficiency. Under this model, injecting a chemical charging power of 1 kW to the battery requires extracting $1/\eta$ kW of electric power from the bus. Similarly, discharging 1 kW of chemical power from the battery injects η kW of electric power to the bus.

The control logic prioritizes using solar power first for the heat pump, then to charge the battery (if the solar supply s exceeds heat pump demand d), then for exports to the rest of the house. If the heat pump demand exceeds the solar supply, the control logic prioritizes powering the heat pump first from the battery, then (if the battery is empty) by importing power from the rest of the house. At each time step, the control logic also ensures that the energy stored at the next time step, x(k+1) in Equation (7), remains above zero and below the energy capacity \bar{x} . Similarly, the control logic ensures that the electric charging power, b(k) from Equation (8), remains above $-\bar{b}$ and below \bar{b} . The control logic can be written concisely as

$$u(k) = \begin{cases} \eta \min\left(s(k) - d(k), \overline{b}, (\overline{x} - ax(k))/((1-a)\tau)\right) & \text{if } s(k) \ge d(k) \\ (1/\eta) \max\left(s(k) - d(k), -\overline{b}, -ax(k)/((1-a)\tau)\right) & \text{otherwise.} \end{cases}$$
(9)

The input signals to the model are the solar power output s and the heat pump demand d. The solar array is modeled on the rooftop PV system at the DC Nanogrid House, which consists of four sub-arrays with the parameters in Table 7. The array has a total nameplate capacity of 14.3 kW DC. The solar power output is simulated using PVLib, an open source Python library [39], and solar irradiance data from the Oikolab weather service. The simulated heat pump is the same unit from the field testing in this paper. It has 14 kW (4 tons) of nameplate cooling capacity. As the laboratory and field test results suggest that the heat pump performance between AC and DC is equivalent within 5 to 10%, which is comparable to the measurement uncertainty range, the simulations use the same historical heat pump power data to represent its electricity demand d on either AC or DC. The simulations also use historical measurements of the rest-of-house AC load, including the auxiliary heating elements. Monthly electric bills are calculated and compared across nanogrid configurations. When solar supply exceeds whole-house demand, the utility is assumed to buy the surplus at the full retail price of 0.14 USD/kWh [40].

5.2. AC and DC nanogrid configurations

Figure 13 shows the three nanogrid configurations modeled here. The first (left) configuration is a typical AC nanogrid that includes PV and battery inverters, a conventional AC bus, and a heat pump. The heat

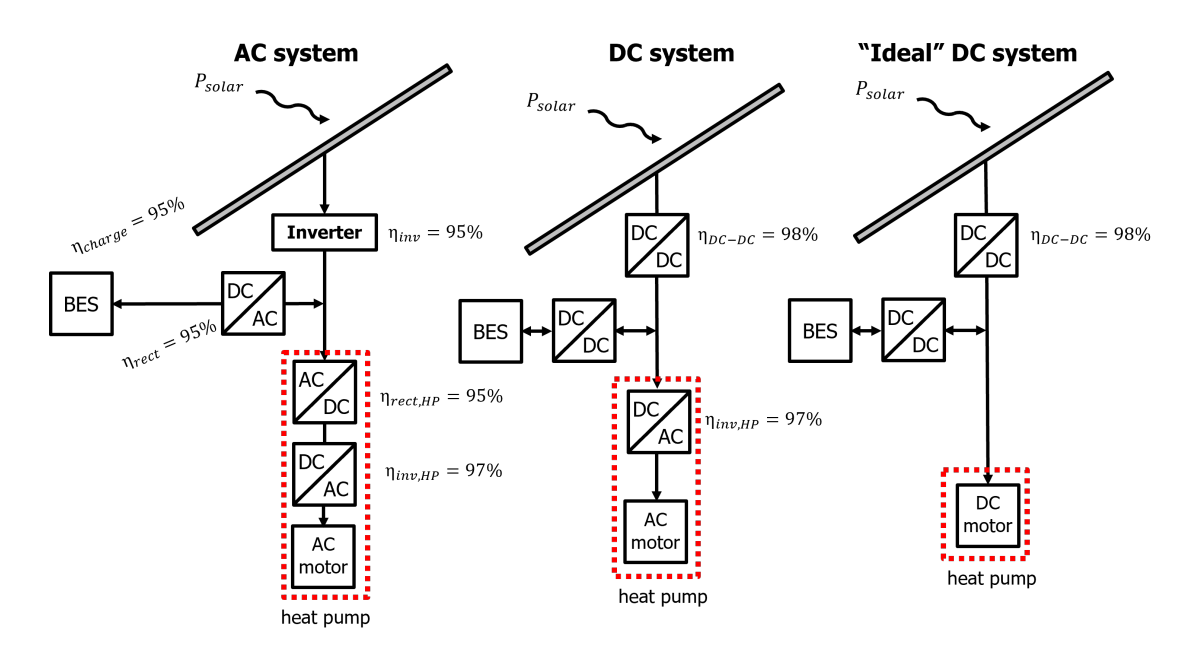


Figure 13: DC nanogrid configuration considering all efficiencies for powering the heat pump, including with a battery.

Table 8: Max converter efficiencies (from Vossos et al. [33])

Component	Peak efficiency [%]
Inverter	95
Rectifier	95
Maximum power-point tracker	98
DC-DC converter	98
Heat pump inverter	97

pump internally rectifies the 60 Hz AC from the bus, then inverts the DC to variable-frequency AC so that the AC motor can drive the compressor at a desired speed. This heat pump configuration represents the hardware that was field-tested at the DC Nanogrid House. The second (center) configuration is similar to the first, but the PV, battery, and heat pump connect on a DC bus. At the heat pump, the DC power bypasses the rectifier and feeds into the same internal inverter depicted in the left configuration. The third (right) configuration is similar to the second, but the heat pump's AC motor is replaced by a DC motor that connects directly to the DC bus. The nanogrid configurations in Figure 13 are based in part on [33]. Converter efficiencies are modeled using the part-load curves illustrated in Figure 14. The peak of each converter's part-load curve was tuned to a value obtained from a manufacturer specification sheet for a representative converter of the same type and cross-checked against the converters used in the real nanogrid. Table 8 shows the peak efficiency for each converter.

5.3. Simulation results

The three nanogrid configurations discussed in Section 5.2 were simulated using the equations and logic from Section 2.3 under coincident hourly data from the calendar year of 2024. Figure 15 shows the monthly electric bills based on simulations that include measured historical power data for the heat pump and the rest-of-house loads, as well as modeled power flows in the nanogrid. Monthly bills are highest in January and February, when heat demand is highest and PV supply is lowest. Winter bills are highest for the AC nanogrid configuration, which has the highest converter losses, and are lowest for the ideal DC configuration. In the summer, the house exports surplus solar power, leading to negative bills (payments from the utility

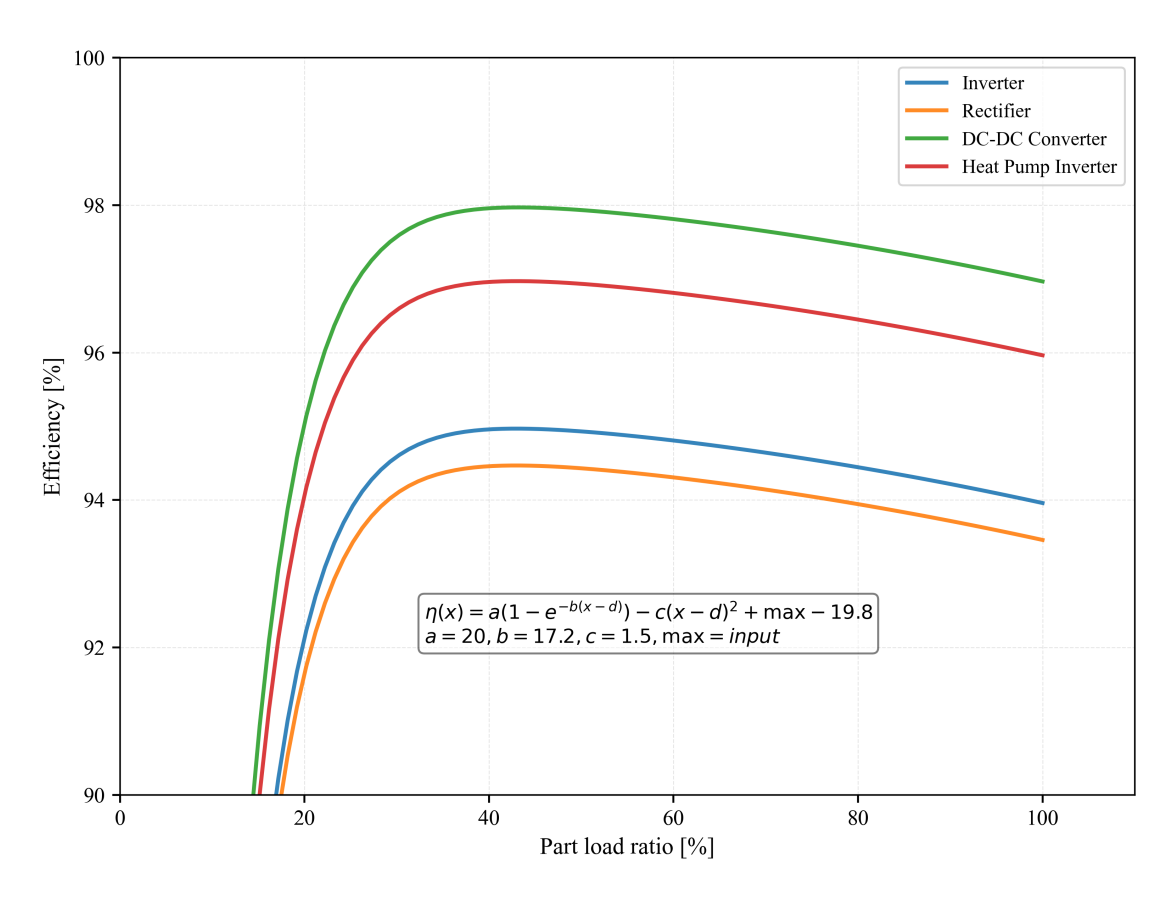


Figure 14: Part-load efficiency curves for each converter in the modeled nanogrid configurations.

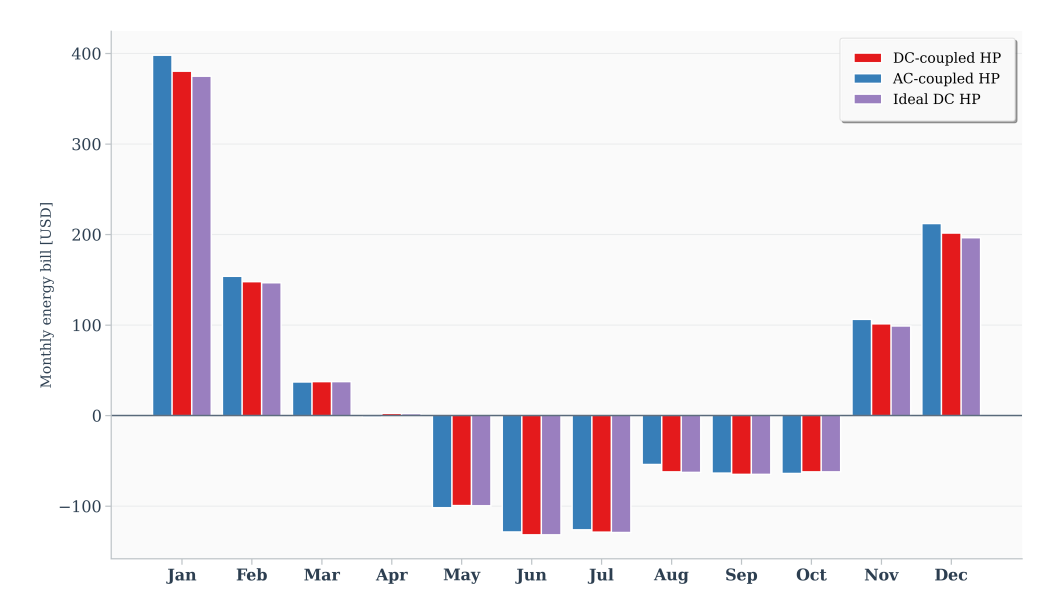


Figure 15: Monthly electricity bills for the test house under the three nanogrid configurations in Figure 13. Electricity bills are highest in winter, when heat demand is highest and PV supply is lowest.

to the house's residents). The payments from the utility are lowest in the AC nanogrid configuration and highest in the ideal DC configuration.

Figure 16 shows the annual electricity bill estimates for the three configurations. The annual bill estimate is highest in the AC configuration (left, 367.4 USD), which has the highest conversion losses. The annual bill estimate for the after-market DC heat pump retrofit that was actually implemented in the test house (center, 321.6 USD) was 12.5% lower than the AC bill estimate. In the ideal DC configuration (right, 306.2 USD), the annual bill estimate was 16.7% lower than the AC bill estimate.

6. Discussion

6.1. Synthesis of results

This study presented three comparisons of AC and DC operation of an off-the-shelf residential unitary air-source heat pump. The first comparison used steady-state laboratory testing under the AHRI Standard 210/240 conditions. The second comparison used field testing in an occupied house with another heat pump of the same make and model as the one tested in the laboratory. The third comparison used modeling of a residential nanogrid with solar PV and a stationary battery. The laboratory tests showed that under steady-state operation, the heat pump performed equivalently under AC and DC within 6%, a range comparable with measurement uncertainty. The COP appeared to be marginally higher on AC at low load, but marginally higher on DC at high load. However, as noted in the sensor accuracy analysis, relative measurement uncertainties were larger at low load. The field tests broadly corroborated the laboratory findings. When comparing heat pump operation on AC vs. DC under similar boundary conditions for one month, the weather-normalized input power was approximately the same to within 10%. This range is again comparable to the measurement uncertainty range, which is somewhat higher for field testing than for laboratory testing.

Although switching the heat pump from AC to DC appeared not to affect performance significantly at the device level, the switch did show efficiency improvements in system-level nanogrid modeling. In simulations, the DC nanogrid configuration reduced annual electricity bills by 12.5% to 16.7%. The lower electricity bills in the DC configurations came from decreasing the number of power conversions and from increasing converter efficiencies (and therefore the battery's round-trip efficiency).

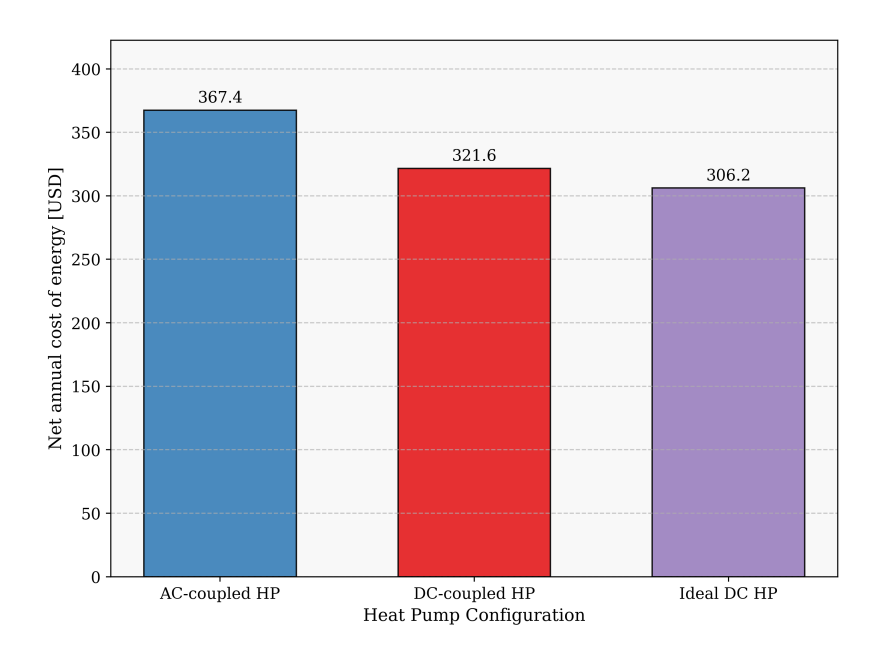


Figure 16: Net annual electricity bill for the test house under the three nanogrid configurations in Figure 13. Annual bills are highest in the AC configuration and lowest in the ideal DC configuration.

For the 208 m², all-electric, detached single-family house in Indiana considered in this study, the estimated annual electricity bill savings from an ideal DC nanogrid configuration, relative to a standard AC configuration, were 61.2 USD. With these annual bill savings, and assuming a simple payback of no more than ten years is required, the highest justifiable capital cost of retrofitting a residential nanogrid to run on DC is 612 USD. While DC retrofit costs are likely to be far higher than this ceiling today, and therefore not justifiable on savings alone, retrofit costs may come down in the future. DC infrastructure may also make financial sense in multifamily retrofits, in new residential construction, or in commercial or industrial buildings.

6.2. Limitations

This paper has several limitations. As previously mentioned, the heat pump compressor drive was not modified to natively accept DC input in the laboratory or field testing. At the manufacturer's recommendation, DC power was simply fed into the same terminals into which AC power would normally connect. On DC, the heat pump internally bypassed its rectifier, feeding the bus's DC power directly to the heat pump's on-board inverter. This could be one source of the differences in the laboratory and field studies, which show the heat pump using slightly more power on DC than on AC in some scenarios. For instance, under DC operation, the bridge-rectifier may have dropped the DC voltage going into the variable-speed drive, decreasing efficiency and potentially accelerating equipment degradation. More detailed testing should be conducted with electrical measurements along the compressor drive to understand the losses which occur between AC and DC power inputs.

A persistent challenge in the field study was normalizing heat pump's performance for differences in weather conditions, occupancy patterns, and possibly equipment degradation between the AC and DC testing. This paper normalized performance data by indoor-outdoor temperature differences, but future work could investigate other normalization methods.

Better modeling of converter part-load efficiencies could refine the system-level nanogrid modeling results. This study used a single, stylized part-load curve for all converters, shifted vertically to model different peak efficiencies for different converters. A more sophisticated approach would tailor each converter's full part-load efficiency curve to data from manufacturer specification sheets or from field measurements. This study also neglected real-world effects in DC microgrids and nanogrids, such as voltage fluctuations, harmonic

effects, load-varying stability, grid interactions, and fault protection. Future work could investigate these effects.

6.3. Future work

Future work could build on this study in at least three ways. First, a nanogrid with, at minimum, a heat pump, a stationary battery, and a PV solar array could be tested in the field. This would allow refined modeling of nanogrid components, experimental investigation of effects that were not modeled here (such as stability, harmonics, and protection), and real-world observation of annual electricity bills. The nanogrid could also be expanded to include an electric vehicle charger or other large loads. Second, after-market DC heat pump conversions could be investigated in more detail. For example, the retrofitted heat pump's variable-speed drive and compressor could be placed on a hot-gas bypass test stand to more thoroughly and precisely evaluate performance. Future work could also test heat pumps with natively DC motors (fixed-speed, two-stage, or variable-speed), rather than the heat pump tested here, which in its default configuration rectified the input AC power then inverted the resulting DC power to a desired frequency in order to govern the compressor speed. Third, field data on DC nanogrid deployment costs could be gathered, enabling cost-benefit analysis and highlighting important areas for innovation.

7. Conclusion

A growing body of simulation research suggests that connecting natively DC devices – such as solar photovoltaics, electric vehicle chargers, stationary batteries, and major appliances driven by DC motors – through DC distribution within buildings could improve energy efficiency. However, this hypothesis remains largely untested in hardware. Toward addressing that gap, this paper tested a major appliance – an airsource heat pump used for space heating and cooling – on AC and DC in the laboratory and the field. As far as the authors are aware, this study reported the first laboratory testing of a DC heat pump retrofit in heating mode, and the first DC heat pump retrofit field testing of any kind. These first-of-a-kind experiments suggested that retrofitting the heat pump from AC to DC did not significantly alter energy efficiency at the device level. However, calibrated year-long system-level modeling suggested that connecting the heat pump to solar photovoltaics and a battery in a DC nanogrid configuration could decrease the test house's annual electricity bills by 12.5% to 16.7%. To the authors' knowledge, these are the first modeling results informed by real-world data from an occupied test house, and therefore constitute a meaningful step toward trustworthy quantification of the benefits of DC distribution systems in residential buildings.

Declaration of Competing Interest

The authors declare that they have no competing financial interests or personal relationships that could have appeared to influence the work reported in this paper.

Declaration of Generative AI and AI-assisted technologies in the writing process

During the preparation of this work the authors used Claude Sonnet 4.0 explicitly for the purpose of formatting matplotlib plots in python. After using this tool, the authors reviewed and edited the content as needed and take full responsibility for the content of the publication. No manuscript writing nor numerical modeling was assisted by any AI-assisted technologies.

CRediT Author Statement

Aaron H.P. Farha: Methodology, Investigation, Software, Visualization, Conceptualization, Writing - Original Draft, Writing - Reviewing and Editing. Jonathan P. Ore: Writing - Reviewing and Editing, Data Curation. Elias N. Pergantis: Methodology, Data Curation, Conceptualization, Reviewing and Editing. Davide Ziviani: Writing - Reviewing and Editing, Conceptualization, Project Administration. Eckhard A. Groll: Writing - Reviewing and Editing, Project Administration, Funding Acquisition. Kevin J. Kircher: Writing - Reviewing and Editing, Visualization, Project Administration, Conceptualization.

Data availability

Data will be made available on request.

Acknowledgments

The Center for High Performance Buildings (CHPB) at Purdue University, USA supported this work. The authors would like to thank the occupants of the DC Nanogrid House for their patience during the field demonstrations. The authors would also like to extend sincere gratitude to Trane Technologies for their technical support throughout the project, especially with regards to the laboratory testing and advising the DC retrofit in the field study.

References

- [1] U.S. Energy Information Administration, Energy consumption by sector (2025). URL http://www.eia.gov/totalenergy/data/monthly/#consumption
- [2] J. Assaf, J. S. Menye, M. B. Camara, D. Guilbert, B. Dakyo, Power converter topologies for heat pumps powered by renewable energy sources: A literature review 13 (19) 3965, publisher: MDPI AG. doi:10.3390/electronics13193965. URL https://www.mdpi.com/2079-9292/13/19/3965
- [3] K. Garbesi, V. Vossos, H. Shen, Catalog of DC appliances and power systems. doi:10.2172/1076790. URL https://www.osti.gov/servlets/purl/1076790/
- [4] A. Stippich, A. Sewergin, G. Engelmann, J. Gottschlich, M. Neubert, From AC to DC: Demonstration of benefits in household appliances.
- V. Vossos, K. Garbesi, H. Shen, Energy savings from direct-DC in U.S. residential buildings 68 223-231, publisher: Elsevier BV. doi:10.1016/j.enbuild.2013.09.009.
 URL https://linkinghub.elsevier.com/retrieve/pii/S0378778813005720
- [6] M. Fotopoulou, D. Rakopoulos, D. Trigkas, F. Stergiopoulos, O. Blanas, S. Voutetakis, State of the art of low and medium voltage direct current (DC) microgrids 14 (18) (2021) 5595.
- [7] E. Rodriguez-Diaz, M. Savaghebi, J. C. Vasquez, J. M. Guerrero, An overview of low voltage DC distribution systems for residential applications, in: 2015 IEEE 5th International Conference on Consumer Electronics-Berlin (ICCE-Berlin), IEEE, 2015, pp. 318–322.
- [8] B. Chen, J. Wang, X. Gu, C. Chen, S. Zhao, Networked microgrids for grid resilience, robustness, and efficiency: A review 12 (1) 18-32, publisher: Institute of Electrical and Electronics Engineers (IEEE). doi:10.1109/tsg.2020.3010570. URL https://ieeexplore.ieee.org/document/9170837/
- [9] C. Charalambous, C. Heracleous, A. Michael, V. Efthymiou, Hybrid AC-DC distribution system for building integrated photovoltaics and energy storage solutions for heating-cooling purposes. a case study of a historic building in Cyprus 216 (2023) 119032. doi:https://doi.org/10.1016/j.renene.2023.119032. URL https://www.sciencedirect.com/science/article/pii/S0960148123009461
- [10] J. Ore, F. Meral, O. Obst, O. Kurtulus, E. A. Groll, Evaluation of a hybrid AC/DC powered residential split-system heat pump performance using a DC nanogrid.
- [11] L. Sriram, A. Farha, A. Hoess, D. Ziviani, E. Groll, E. Pergantis, K. Kircher, Development and comparative analysis of a power-over-ethernet (PoE) DC lighting system for residential buildings.
- [12] R. Chacko, A. Thevarkunnel, Z. Lakaparampil, J. Thomas, DC nanogrid for buildings: Study based on experimental investigation of load performance and annual energy consumption 58 352-358, publisher: Elsevier BV. doi:10.1016/j.matpr.2022.02.267.
 URL https://linkinghub.elsevier.com/retrieve/pii/S2214785322009002
- [13] N. R. Watson, J. D. Watson, An overview of HVDC technology 13 (17) (2020) 4342.
- [14] W. Wang, G. Li, J. Guo, Large-scale renewable energy transmission by HVDC: Challenges and proposals 19 (2022) 252–267.
- [15] M. Shahidehpour, X. Liu, Z. Li, Y. Cao, Microgrids for enhancing the power grid resilience in extreme conditions 1–1Publisher: Institute of Electrical and Electronics Engineers (IEEE). doi:10.1109/tsg.2016.2579999.
 URL http://ieeexplore.ieee.org/document/7489002/
- [16] F. Dastgeer, H. E. Gelani, H. M. Anees, Z. J. Paracha, A. Kalam, Analyses of efficiency/energy-savings of DC power distribution systems/microgrids: Past, present and future 104 89–100, publisher: Elsevier BV. doi:10.1016/j.ijepes.2018.06.057. URL https://linkinghub.elsevier.com/retrieve/pii/S0142061518305623
- [17] F. Dastgeer, H. E. Gelani, A comparative analysis of system efficiency for AC and DC residential power distribution paradigms 138 648-654, publisher: Elsevier BV. doi:10.1016/j.enbuild.2016.12.077. URL https://linkinghub.elsevier.com/retrieve/pii/S0378778816320461
- [18] T. Dragicevic, X. Gu, J. C. Vasquez, J. M. Guerrero, DC microgrids—part II: A review of power architectures, applications, and standardization issues 31 (5) 3528–3549, publisher: Institute of Electrical and Electronics Engineers (IEEE). doi:10.1109/tpel.2015.2464277.
 - URL http://ieeexplore.ieee.org/document/7177102/

- [19] R. K. Chauhan, F. Gonzalez-Gongatt, B. S. Rajpurohit, S. N. Singh, DC microgrid in residential buildings, Institution of Engineering and Technology, pp. 367–388. doi:10.1049/pbpo115e_ch15. URL https://digital-library.theiet.org/content/books/10.1049/pbpo115e_ch15
- [20] A. T. Elsayed, A. A. Mohamed, O. A. Mohamed, DC microgrids and distribution systems: An overview 119 407-417, publisher: Elsevier BV. doi:10.1016/j.epsr.2014.10.017. URL https://linkinghub.elsevier.com/retrieve/pii/S0378779614003885
- [21] D. Lorusso, S. Mlyniec, J. Casey, Introduction to fault-managed power, in: 2025 IEEE International Symposium on Product Compliance Engineering (ISPCE), IEEE, 2025, pp. 1–6.
- [22] J. P. Ore, E. A. Groll, Analysis of a residential house for the design and implementation of a DC nanogrid, in: 2020 IEEE PES Innovative Smart Grid Technologies Europe (ISGT-Europe), IEEE, pp. 749-753. doi:10.1109/isgt-europe47291.2020.9248788. URL https://ieeexplore.ieee.org/document/9248788/
- [23] J. Ore, F. Meral, D. Ziviani, E. Groll, The case for DC: Motivation of modern topologies, DC-powered solutions, and applications within residential environments.
- [24] J. P. Ore, The DC Nanogrid House: Converting a residential building from AC to DC power to improve energy efficiency, Ph.D. thesis, Purdue University (2021).
- [25] E. N. Pergantis, N. Al Theeb, P. Dhillon, J. P. Ore, D. Ziviani, E. A. Groll, K. J. Kircher, et al., Field demonstration of predictive heating control for an all-electric house in a cold climate 360 (2024) 122820.
- [26] E. N. Pergantis, P. Dhillon, L. D. R. Premer, A. H. Lee, D. Ziviani, K. J. Kircher, Humidity-aware model predictive control for residential air conditioning: A field study 266 (2024) 112093.
- [27] E. N. Pergantis, L. D. R. Premer, A. H. Lee, H. Liu, E. A. Groll, D. Ziviani, K. J. Kircher, et al., Protecting residential electrical panels and service through model predictive control: A field study 386 (2025) 125528.
- [28] V. Vossos, D. L. Gerber, M. Gaillet-Tournier, B. Nordman, R. Brown, W. Bernal Heredia, O. Ghatpande, A. Saha, G. Arnold, S. M. Frank, Adoption pathways for DC power distribution in buildings 15 (3) 786, publisher: MDPI AG. doi:10.3390/en15030786.
 URL https://www.mdpi.com/1996-1073/15/3/786
- [29] D. Fregosi, S. Ravula, D. Brhlik, J. Saussele, S. Frank, E. Bonnema, J. Scheib, E. Wilson, A comparative study of DC and AC microgrids in commercial buildings across different climates and operating profiles, in: 2015 IEEE First International Conference on DC Microgrids (ICDCM), IEEE. doi:10.1109/icdcm.2015.7152031. URL http://ieeexplore.ieee.org/document/7152031/
- [30] H. Kakigano, M. Nomura, T. Ise, Loss evaluation of DC distribution for residential houses compared with AC system, in: The 2010 International Power Electronics Conference - ECCE ASIA -, IEEE. doi:10.1109/ipec.2010.5543501. URL http://ieeexplore.ieee.org/document/5543501/
- [31] B. Muruganantham, R. Gnanadass, N. Padhy, Challenges with renewable energy sources and storage in practical distribution systems 73 125-134, publisher: Elsevier BV. doi:10.1016/j.rser.2017.01.089. URL https://linkinghub.elsevier.com/retrieve/pii/S1364032117301004
- [32] A. Frances, R. Asensi, O. Garcia, R. Prieto, J. Uceda, Modeling electronic power converters in smart DC microgrids—an overview 9 (6) 6274–6287, publisher: Institute of Electrical and Electronics Engineers (IEEE). doi:10.1109/tsg.2017.2707345.
- doi:10.1109/tsg.2017.2707345.

 URL https://ieeexplore.ieee.org/document/7932955/

 [33] V. Vossos, S. Pantano, R. Heard, R. Brown, DC appliances and DC power distribution: A bridge to the future net zero
- energy homes (2017).

 URL https://publications.europa.eu/en/publication-detail/-/publication/a270a15c-fb38-11e7-b8f5-01aa75ed71a1/language-en
 [34] K. Garbesi, V. Vossos, A. Sanstad, G. Burch, Optimizing energy savings from direct-DC in U.S. residential buildings.
- [35] C. B. Nzoundja Fapi, M. L. Touré, M.-B. Camara, B. Dakyo, Control strategy for DC micro-grids in heat pump applications with renewable integration 14 (1) 150, publisher: MDPI AG. doi:10.3390/electronics14010150.
 URL https://www.mdpi.com/2079-9292/14/1/150
- [36] American Heating, Air-Conditioning and Refrigeration Institute, Performance rating of unitary air-conditioning & air-source heat pump equipment, AHRI Standard 210/240 (2023).
- [37] E. N. Pergantis, A. S. Sangamnerkar, O. J. Priyadarshan, P. Dhillon, D. Ziviani, E. A. Groll, K. J. Kircher, Sensors, storage, and algorithms for practical optimal controls in residential buildings 129 (2023) 437–444.
- [38] American Society of Heating, Refrigeration, and Air-Conditioning Engineers, Climatic data for building design standards, ASHRAE Standing Project Committee 169 (2020).
- [39] K. S. Anderson, C. W. Hansen, W. F. Holmgren, A. R. Jensen, M. A. Mikofski, A. Driesse, PVlib python: 2023 project update 8 (92) 5994, publisher: The Open journaltitle. doi:10.21105/joss.05994. URL https://joss.theoj.org/papers/10.21105/joss.05994
- [40] Duke Energy Indiana, Residential rates (2025). URL https://www.duke-energy.com/